

## Fast Bound Pool Fraction mapping via steady-state MT saturation using single-shot EPI

Marco Battiston<sup>1</sup>, Torben Schneider<sup>2</sup>, Francesco Grussu<sup>1,3</sup>, Marios Yiannakas<sup>1</sup>, Ferran Prados<sup>1,4,5</sup>, Claudia A.M. Gandini Wheeler-Kingshott<sup>1,6</sup>, and Rebecca S. Samson<sup>1</sup>

<sup>1</sup>Queen Square MS Centre, Department of Neuroinflammation, UCL Queen Square Institute of Neurology, Faculty of Brain Sciences, UCL, London, United Kingdom, <sup>2</sup>Philips UK, Guilford, United Kingdom, <sup>3</sup>Centre for Medical Imaging Computing, Department of Computer Science, UCL, London, United Kingdom, <sup>4</sup>Centre for Medical Imaging Computing, Department of Medical Physics and Biomedical Engineering, UCL, London, United Kingdom, <sup>5</sup>Universitat Oberta de Catalunya, Barcelona, Spain, <sup>6</sup>Department of Brain and Behavioural Sciences, University of Pavia, Pavia, Italy

### Synopsis

The bound pool fraction (*BPF*) is a quantitative parameter that reflects macromolecular tissue fraction, and has shown sensitivity to myelin content in human white matter. *BPF* mapping is still largely unexploited for characterizing white matter disease in vivo due to the long MRI protocols needed for its accurate and precise computation. In this work, we develop a new method that allows fast unbiased *BPF* estimation, suitable for clinical applications.

### Introduction

The bound pool fraction (*BPF*) is a key biophysical parameter for quantifying the magnetization transfer (MT) effect, as it describes the fraction of macromolecular protons undergoing chemical exchange and cross-relaxation with protons in mobile water molecules. The *BPF* has been associated with tissue macromolecular content, and has shown correlation with myelin content in the central nervous system<sup>1</sup>, hence the interest in developing methods to robustly extract this parameter in vivo.

*BPF* mapping for clinical applications remains challenging given the complexity of the two-pool model<sup>2</sup> used for its estimation. Existing fast methods rely on fixing unknown model parameters to population average values<sup>3,4</sup>, which may introduce bias when deviating from the healthy condition.

Here, we develop a new approach for fast *BPF* mapping. Hard constraints adopted in previous methods are relaxed by using approximations on the two-pool model that can be invoked under: (i) steady-state conditions, and (ii) “fast-exchange” regime conditions. A single-shot spin-echo (ssh-SE-) EPI sequence is adapted to accommodate (i) and (ii), giving an acquisition time of under 10 minutes.

### Methods

In the fast-exchange regime, bound and free protons exchange magnetization with a time scale much shorter than spin-lattice relaxation<sup>5</sup>. This allows the steady-state signal under off-resonance saturation to be expressed as<sup>6</sup>:

$$\frac{M_{ss}(\Delta, \theta)}{M_0} = \frac{1 - (\delta_B BPF) e^{-\frac{PRT}{T_1}}}{1 - (1 - \delta_B BPF) e^{-\frac{PRT}{T_1}}} \quad [1]$$

assuming that: (i) pulse repetition time (*PRT*) is long compared to transfer time (i.e.  $PRT > 120\text{ms}^7$ ); (ii) off-resonance saturation does not affect the free pool (i.e. offset frequency  $\Delta > 2\text{kHz}$ ); (iii) bound pool saturation (expressed by  $\delta_B$  in Equation 1) takes place instantaneously (i.e. no exchange or relaxation during off-resonance saturation).  $M_{ss}$ , as a function of  $\Delta$  and saturation flip angle  $\theta$ , can be fitted to extract *BPF* and bound pool  $T_2$  ( $T_2^B$ ), given an external measure of  $T_1$ .

Time-efficient sampling of the steady-state is achieved using the sequence shown in Figure 1. The pulsed steady-state is attained with an initial period of saturation, and maintained during the acquisition of  $N_s$  slices with ssh-SE-EPI readouts. Short recovery times between sequence repetitions are allowed, as the steady-state established by the subsequent preparation is independent from the magnetization initial state.

The effect of sequence parameters and number of data points is investigated through simulations. Full two-pool model equations are used to generate steady-state signals for physiologically plausible value of tissue parameters, then fitted by Equation 1. Error on parameter estimates is evaluated for protocols of Figure 2. In vivo acquisition is performed using the optimized protocol O1. A FOV of  $224 \times 224 \times 120\text{mm}^3$  at  $2\text{mm}^3$  isotropic resolution is acquired with ssh-SE-EPI readouts for: (i) MT steady-state; (ii) Inversion Recovery (IR) for  $T_1$  mapping; and (iii) Double-Angle Method (DAM) for  $B_1$  mapping<sup>8</sup>. Total protocol duration: 8min 44sec. A 3D- $T_1$ -weighted scan is added to allow regional characterization of the *BPF*. Six healthy subjects are scanned on a 3T Philips Ingenia CX MRI.

### Results

The effect of sequence parameters and number of data points on parameters estimation is shown in Figure 3. The use of long  $PRT > 100\text{ms}$  is necessary to ensure the validity of model approximations. Shorter  $PRT$ s in fact produce large bias on *BPF*, even at high SNR. The *BPF* is estimated more reliably than  $T_2^B$ , however precision and accuracy of both parameters deteriorate at low SNR $\sim 15$ , regardless the number of data point used. Protocol optimization reduces parameters errors enabling the sampling of less data points.

In vivo *BPF* maps depict the expected contrast, as shown in Figure 4 for a representative subject. Average values in WM and GM are in agreement with literature values<sup>3</sup>, with population median WM/GM *BPF* of 0.114/0.068. *BPF* distributions from all subjects pooled together are shown in Figure 5, displaying similar patterns of previous studies<sup>9</sup>.

## Discussion

The method developed efficiently exploits the fast-exchange regime approximation for the steady-state MT, where off-resonance saturation is applied at long  $PRT$ , by acquiring the entire  $k$ -space between saturation pulses. This produces an MT-weighted volume per  $TR \sim 15$ -20seconds. The interference of a multi-slice readout on the MT steady-state is reduced by avoiding fat suppression pulses and adopting an interleaved slice order in the acquisition. However, further investigation is required to quantify any residual effect, as well as to assess the impact of different pulse shape and/or duration.

The negligible  $BPF$  bias, the lack of explicit constraints on model parameters, and the short scan time needed are promising factors for the translation of the method to clinical applications.

## Conclusions

A new, fast approach to map a key parameter of the quantitative MT two-pool model has been developed and applied in a cohort of healthy volunteers. The approach has the potential to be applied in a patient population in clinical studies.

## Acknowledgements

UK Multiple Sclerosis Society. Spinal Research (UK), Wings for Life (Austria) and Craig H. Neilsen Foundation (USA) for INSPIRED. Engineering and Physical Sciences Research Council (EPSRC EP/R006032/1, M020533/1, G007748, I027084, M020533, N018702). Department of Health's National Institute for Health Research, Biomedical Research Centres (BRC R&D 03/10/RAG0449). Guarantors of Brain post-doctoral non-clinical fellowships. This project has received funding from the European Union's Horizon 2020 research and innovation programme under grant agreement No. 634541.

## References

[1] Schmierer, Klaus, et al. "Quantitative magnetization transfer imaging in postmortem multiple sclerosis brain." *Journal of Magnetic Resonance Imaging* 26.1 (2007): 41-51; [2] Henkelman, R. Mark, et al. "Quantitative interpretation of magnetization transfer." *Magnetic resonance in medicine* 29.6 (1993): 759-766; [3] Yarnykh, Vasily L. "Time-efficient, high-resolution, whole brain three-dimensional macromolecular proton fraction mapping." *Magnetic resonance in medicine* 75.5 (2016): 2100-2106; [4] Dortch, Richard D., et al. "Optimization of selective inversion recovery magnetization transfer imaging for macromolecular content mapping in the human brain." *Magnetic resonance in medicine* (2018); [5] Helms, Gunther. "Interaction of exchange and differential relaxation in the saturation recovery behavior of the binary spin-bath model for magnetization transfer." *Concepts in Magnetic Resonance Part A* 28.4 (2006): 291-298; [6] Helms, Gunther, and Andreas Piringer. "Simultaneous measurement of saturation and relaxation in human brain by repetitive magnetization transfer pulses." *NMR in Biomedicine* 18.1 (2005): 44-50; [7] Soellinger, M., et al. "Fast bound pool fraction mapping using stimulated echoes." *Magnetic resonance in medicine* 66.3 (2011): 717-724; [8] Stollberger, Rudolf, and Paul Wach. "Imaging of the active B1 field in vivo." *Magnetic Resonance in Medicine* 35.2 (1996): 246-251; [9] Mchinda, Samira, et al. "Whole brain inhomogeneous magnetization transfer (ihMT) imaging: Sensitivity enhancement within a steady-state gradient echo sequence." *Magnetic resonance in medicine* 79.5 (2018): 2607-2619; [10] Alexander, Daniel C. "A general framework for experiment design in diffusion MRI and its application in measuring direct tissue-microstructure features." *Magnetic Resonance in Medicine* 60.2 (2008): 439-448; [11] Cardoso, M. Jorge, et al. "Geodesic information flows: spatially-variant graphs and their application to segmentation and fusion." *IEEE transactions on medical imaging* 34.9 (2015): 1976-1988.

## Figures

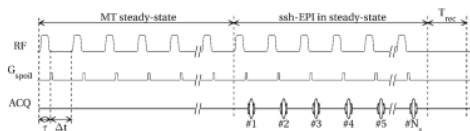


**Figure 1:** An off-resonance pulse is repeated every  $PRT = \tau + \Delta t$  (where  $\tau \Delta t$  refer to the pulse duration/interval), for a time period sufficient to build a steady-state (typically  $> 3s$ ). To exploit model approximations necessary to derive Equation 1,  $PRT$  has to be  $> 120ms$ . This allows us to fit a ssh-EPI module in between pulses, enabling high time-efficiency in the acquisition while maintaining the steady-state. Fat suppression is performed using the gradient reversal technique, and inter-slice MT effects are reduced adopting an interleaved slice acquisition order. A short recovery time  $T_{rec} \ll 5T_1$  is allowed, as the magnetization will be forced into a new steady-state.

Simulations						
protocol	# data point	$\tau$ [ms]	$\Delta t$ [ms]	pulse shape	$\theta$ [°]	$\Delta$ [kHz]
L1	20	6	44	fermi	000/000/000/000/000/000 070/070/070/070/070/070 700/700/700/700/700/700	0.000/0.070/0 3.250/0.000/0.010 0.000/0.000/0.000
L2	20	6	94	fermi	000/000/000/000/000/000 070/070/070/070/070/070 700/700/700/700/700/700	0.000/0.070/0 3.250/0.000/0.010 0.000/0.000/0.000
L3	20	6	144	fermi	000/000/000/000/000/000 070/070/070/070/070/070 700/700/700/700/700/700	0.000/0.070/0 3.250/0.000/0.010 0.000/0.000/0.000
L4	20	6	194	fermi	000/000/000/000/000/000 070/070/070/070/070/070 700/700/700/700/700/700	0.000/0.070/0 3.250/0.000/0.010 0.000/0.000/0.000
S1	8	6	144	fermi	070/070/070 700/700/700/700	0.000/0.070/0 3.250/0.000/0.010
O1	10	8	142	fermi	000/000/000/000/000/000 070/070/070/070/070/070 700/700/700/700/700/700	0.000/0.070/0 3.250/0.000/0.010 0.000/0.000/0.000
In vivo						
MT protocol: 01 + 2M <sub>0</sub> volumes		T <sub>1</sub> protocol: IR-EPI		B <sub>1</sub> protocol: DAM-EPI		
FOV: 240x240x12 mm <sup>3</sup>		FOV: 240x240x12 mm <sup>3</sup>		FOV: 240x240x12 mm <sup>3</sup>		
resolution: 2x2x2 mm <sup>3</sup>		resolution: 2x2x2 mm <sup>3</sup>		resolution: 2x2x2 mm <sup>3</sup>		
TE/TR: 38 ms/16890ms		TE/TR: 43 ms/6735ms		TE/TR: 38 ms/12000ms		
T <sub>rec</sub> : 1800 ms		TE: 50ms to 1730ms (15)		$\alpha_1/\alpha_2$ : 60°/120°		
SENSE factor :2		SENSE /MB factor :2/2		SENSE : 2		
bandwidth: 575 kHz		bandwidth: 575 kHz		averages: 2		

**Figure 2:** Details of protocols used for simulations (long protocols L1, L2, L3 and L4, short protocol S1, and optimized protocol O1), and imaging parameters used for in vivo acquisition, for which O1 was chosen. The optimized protocol is obtained by minimization of Cramer-Rao lower bounds<sup>10</sup> for both  $BPF$  and  $T_2^B$ . Details of IR-EPI for  $T_1$  mapping, and DAM-EPI for  $B_1$  mapping are also reported.

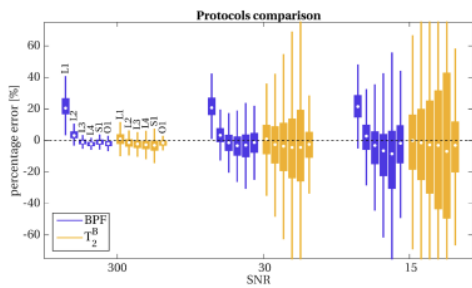


**Figure 3:** Distributions of estimate errors on model parameters  $BPF$  and  $T_2^B$  for the protocols defined in Figure 2: four versions of long (L) protocols, one short (S) protocol, and one optimized (O) protocol using Cramer-Rao lower bounds optimization are considered. Errors are evaluated at different SNR=300, 30 and 15, with SNR=30 representing the hypothetical in vivo acquisition scenario.

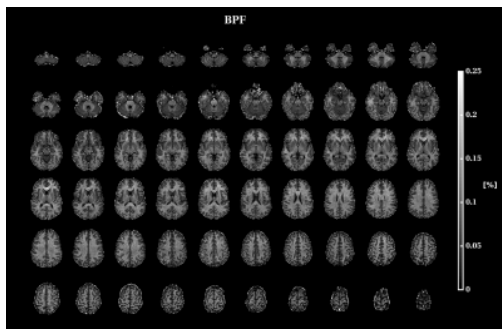


**Figure 4:** Example of  $BPF$  map in a representative subject. Maps are acquired at  $2\text{mm}^3$  isotropic resolution covering  $12\text{cm}^3$  in the foot-head direction. The total scan time to obtain these maps, including  $T_1$  mapping and  $B_1$  correction, is 8min 44sec. The expected WM/GM contrast is appreciable throughout the whole acquired volume.

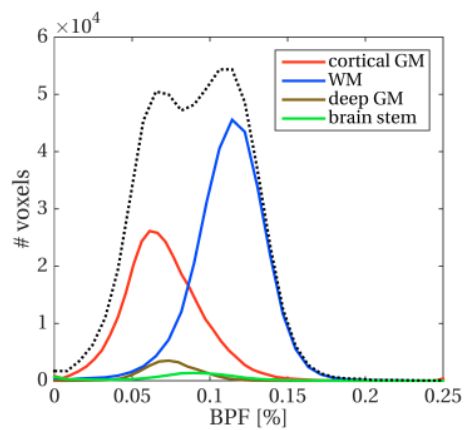


**Figure 5:**  $BPF$  distribution for all subjects pooled together (dashed black line), and underlying tissue type distributions (cortical grey matter in red, white matter in blue, deep grey matter in brown, and brain stem in green). Different brain regions are obtained using the GIF<sup>11</sup> segmentation tool on the  $3D-T_1$ -weighted volume registered to the subject-specific EPI space. The whole population  $BPF$  displays a bi-modal distribution driven by WM and cortical GM peaks, respectively at 0.114(0.100-0.128 25<sup>th</sup>-75<sup>th</sup> percentiles) and 0.068 (0.054-0.085 25<sup>th</sup>-75<sup>th</sup> percentiles).